HiSST: 3rd International Conference on
High-Speed Vehicle Science Technology
14 -19 April 2024, Busan, Korea

Numerical Study on Heat Fluxes in Hypersonic Flow over a 3D Sharp Cone

Soham Sinha[1], Mohammed Ibrahim Sugarno[2]

Abstract

The conical nose shape has long been a focal point of high-speed aerodynamic research. It serves as the foundation from which a multitude of general forebody designs, including waveriders, draw their inspiration. Beyond its inherent simplicity, the flow dynamics around this body are particularly amenable to analysis due to the inherently conical nature of the flow. This study aims in investing the change in flow physics over a sharp cone as the angle of attack (AoA) is changed. Due to this alteration, the heat transfer rate to the conical surface from the windward side to the leeward side will also get affected. The model used here is a 200mm slender cone with 8° semi-apex angle having a sharp leading edge. The free-stream conditions used for the study corresponds to Hypersonic Shock Tunnel facility at Hypersonic Experimental Aerodynamics Laboratory (HEAL) at Indian Institute of Technology Kanpur. The simulations will be done for Mach 6 with variable AoA. The notable flow features are change in shock angle, heat flux to the conical surface and the recirculation zone at the base of the cone with variation of AoA. Laminar model is used for the flow over the cone. So, it will give an idea about the heat flux if the entire flow over the conical body can be maintained laminar. Work is in progress and numerical results will be presented.

Keywords: Hypersonic Laminar Conical flow, Heat Flux, Shock Angles, Different Angle of Attacks, Recirculation Zone.

Nomenclature

P_∞	Freestream Pressure	P_0	Stagnation Pressure
M_∞	Freestream Mach Number	P_{driver}	Pressure in the driver section
T_∞	Freestream Temperature	H_0	Stagnation Enthalpy
α	Angle of Attack(degrees)	T_{wall}	Wall Temperature
Φ	Circumferential Axis(degrees)	T_0	Stagnation Temperature

1. Introduction

The prevalent forebody configuration in numerous hypersonic vehicles and weapon systems is the cone shape. Although this design exhibits a simple geometry, the aerodynamic phenomena it generates during hypersonic flight, particularly at moderate to high angles of attack, can be remarkably intricate. These complexities encompass phenomenon such as boundary layer separation on the smooth surface, the formation of vortices on the leeward side, and the intricate interplay of secondary shockwaves. Conversely, when a sharp cone encounters hypersonic flow at a zero angle of attack, the scenario is notably simplified. This entails the presence of an attached conical shockwave in conjunction with the development of an attached boundary layer on the surface. This boundary layer can exhibit varying characteristics, transitioning from laminar to transitional or turbulent flow regimes. Complexity starts developing on increasing angle of attack as the shock layer on the windward side reduces in thickness

1 Masters of Technology Student, Indian Institute of Technology Kanpur, sohamsinha22@iitk.ac.in
2 Associate Professor, Indian Institute of Technology Kanpur, ibrahim@iitk.ac.in

along with developing cross flow around the cone resulting in variable pressure distribution and heat flux in the axial and circumferential direction. As the surface pressure on the leeward side becomes adverse, the boundary layer tends to separate giving rise to leeside vortex system due rolling up of shear layers in viscous flow. Secondary internal shocks can also build up depending on the angle of attack and Mach number. The sharp leading edge of the cone removes the possibility of detached bow shock which may impose strong adverse axial pressure gradient at the nose leading to flow separation. If separation occurs at large angle of attacks, high heating rates can be observed on increasing the angle of attack.

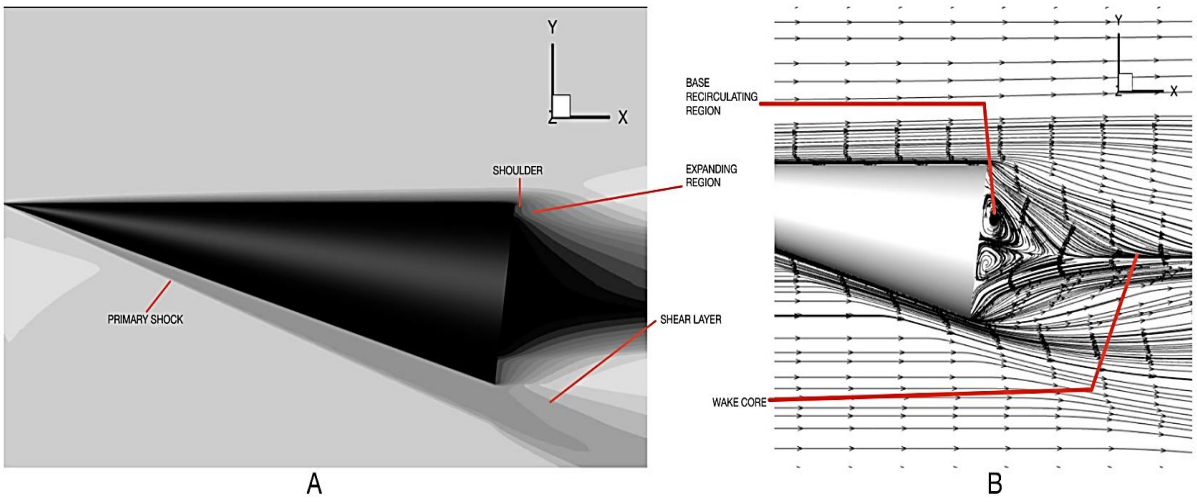

Fig 1. Mach Number Gradients within hypersonic flow over cone (A) and Flow Streamlines (B)

The objective of this research is to experimentally simulate high enthalpy hypersonic flow over a sharp cone, with a primary focus on comprehending the following aspects:

- The notable flow feature transitions from windward side to the leeward side over the cone with change in angle of attack.
- The influence of changes in the angle of attack on the heat transfer rate experienced by the cone's surface.
- The impact of the recirculation zone on the heat transfer rate at the base of the cone.

2. Literature Review

Taylor and Maccoll[2] pioneered early methods for predicting inviscid 3D flow around sharp-nosed cones at supersonic and hypersonic speeds. Subsequently, Van Dyke[7] developed an analytical solution for hypersonic flow by linearizing the Taylor-Maccoll equation, providing accurate results for high Mach numbers and small cone angles, which was later extended by Rasmussen[4] to include unyawed cones. Stone's[6] improvements to zero angle of attack solutions were further refined by Kopal[9] and Sims[8] for small angle of attack scenarios. However, Stone's perturbation theory contradicts the steady inviscid adiabatic flow's energy equation, highlighting Ferri's[5] study that emphasizes varying entropy jumps due to shockwave curvature, particularly at high angles of attack, with the emergence of a vortical singularity region and a vortical layer near the cone surface. Cheng[10] utilized Newtonian Impact theory to approximate analytical solutions to Stone's problem, while Doty[11] and Rasmussen[4] derived analytical solutions beyond Newtonian constraints, accurately interpreting outer flow over inclined cones in hypersonic conditions. Recent advances in high-fidelity Computational Fluid Dynamics (CFD) have enabled the prediction of viscous effects, surface heat transfer, and pressures, though matching experimental results for cases with intense heat-transfer rates remains challenging due to mesh generation and proper modeling ambiguities resulting in multiple solutions.

3. Numerical Analysis

Computational Fluid Dynamics numerically solves the governing flow equations to predict flow properties around bodies, employing iterative processes on computers with specified initial conditions. The Navier-Stokes equations serve as the primary governing equations and are often solved using the Finite Volume Method. This method involves discretizing domains into cells, applying Gauss divergence theorem, and ensuring conservation of mass, momentum, and energy within each cell. In this study, we employ numerical simulations using Ansys Fluent to gain insights into the flow phenomena surrounding the cone. The simulations are conducted under two distinct conditions: one with a Mach 6 shock tunnel mode and a stagnation flow enthalpy of approximately 1.1 MJ/Kg, and the other with a stagnation flow enthalpy of 2.0 MJ/Kg. For each of these stagnation enthalpy settings, the angle of attack of the cone is varied from 0° to 8° in step of 4°. The freestream conditions used for the simulation are given in Table 1 as referred for shock tunnel with Helium as driver gas [14]. This analysis allows us to establish an initial understanding of the dynamic behavior within the flow field surrounding the cone.

Table 1. Freestream Conditions used for the study

Flow Type	Low Enthalpy	High Enthalpy
H_0 (KJ/Kg)	1.1	2.0
T_0 (K)	1104.086	2029.276
T_∞(K)	447.863	823.158
P_0(KPa)	549.6	1635.152
P_∞(KPa)	0.5442	1.6192
P_{driver}(Kpa)	$1*10^3$	$3*10^3$
M_∞	6	6

3.1 Geometry

The simulation setup features a 3D cone model with a length, L = 200mm and a semi-apex angle of 8° in accordance with the model used in HEAL, IIT Kanpur. The computational domain extends 0.75L upstream from the apex of the cone and L downstream from the base of the cone. In cross stream direction, the domain extends to 0.75L on either side from the axis of the cone. The dimensions of the domain are fixed based on the dimensions of the test section of the shock tunnel present in HEAL, IIT Kanpur. Due to this the blockage ratio is 2.75%(approx.).

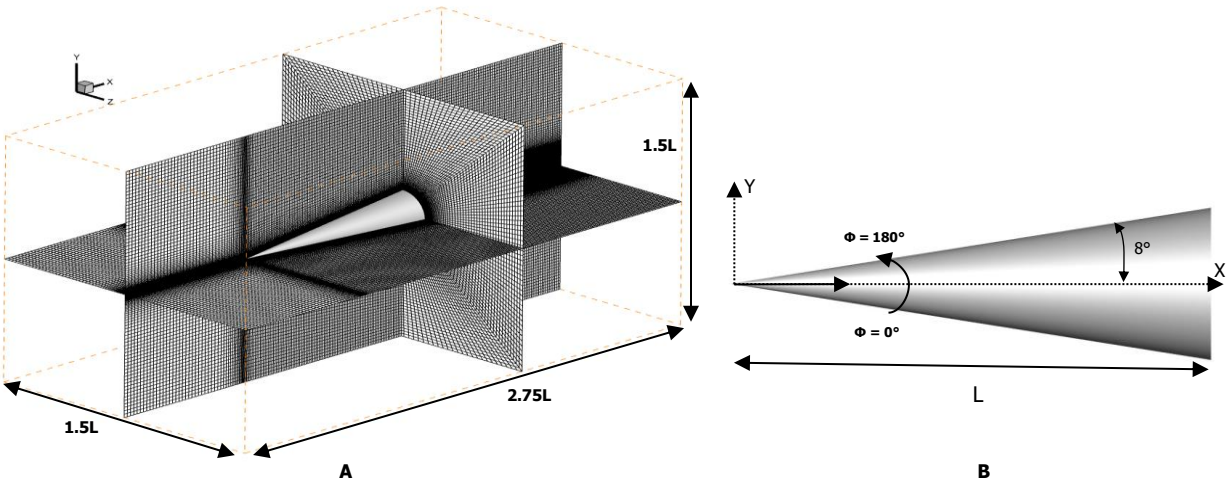

Fig 2. Physical Domain showing the Mesh (A) and Schematic diagram of cone showing the flow directions from left to right (B)

3.2 Grid Generation

A structured mesh was created using ICEM CFD (Fig 2.A) for the sharp cone case due to its inherent simplicity. Utilizing a structured mesh offered numerous advantages, notably enhanced computing efficiency, as the alignment of cells with the flow was improved. The quality of the mesh was assessed using two criteria, angle, and determinant (2x2x2), and smoothing was performed to ensure 99% of the cells has a determinant greater than 0.4 and angle of at least 18°.

3.3 CFD Model Used

Simulations were conducted using both the Laminar and Spalart-Allmaras models for an Ideal gas employing a density-based solver. Comparative analysis of the results from both simulations indicated negligible differences for both α = 4°(Fig 3.A) and α = 8°(Fig 3.B), leading to the selection of the Laminar model. This decision was also taken to look into the flow physics if the entire flow over the cone can be maintained laminar considering the small length of the cone.

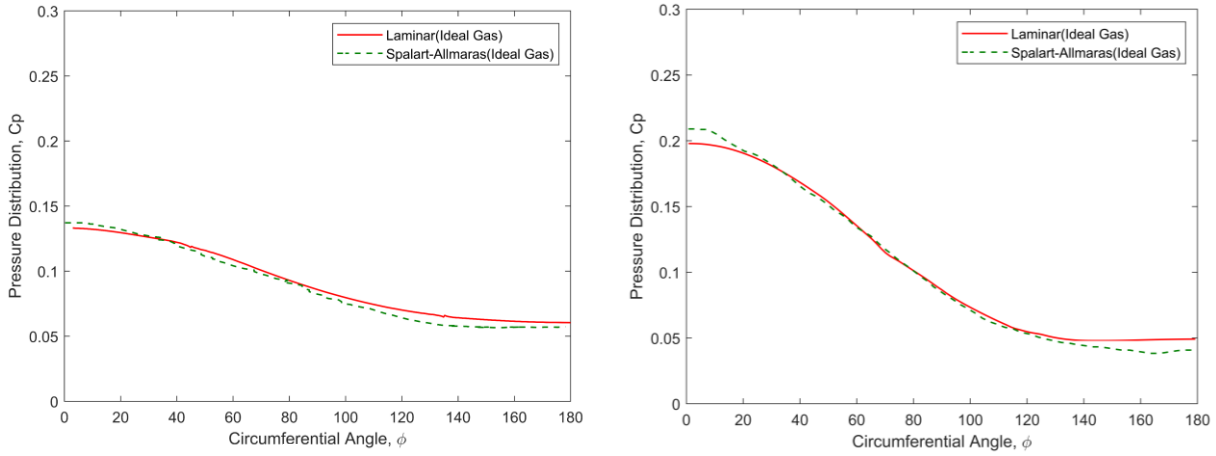

A **B**

Fig 3. Comparison between Laminar Model and Spalart-Allmaras Model for α = 4°(A) and α = 8°(B)

3.4 Boundary Conditions

No-slip wall boundary conditions were applied to the cone slant surface, the sting surface, and the computational wall domain, with no roughness effects considered. The entire cone surface was uniformly assigned a wall temperature of 300K, establishing an isothermal condition for the simulation. The inlet was designated as a pressure farfield boundary condition, defining constant Mach number, static pressure, and temperature based on the values provided in Table 1. Finally, the outlet boundary condition was specified as a pressure outlet, maintaining fixed outlet static pressure and temperature equivalent to the freestream values.

3.5 Grid Convergence

A grid convergence study was done for the sharp cone at 4° AoA using circumferential pressure distribution at 85mm axial distance from the apex of the cone. Three grids are generated as follows:

Table 2. Grid Convergence

Grid Type	Total Nodes	Maximum Pressure (Pa)
Coarse	4799080	5.43514e+03
Medium	6601485	5.42895e+03
Fine	8088475	5.42977e+03

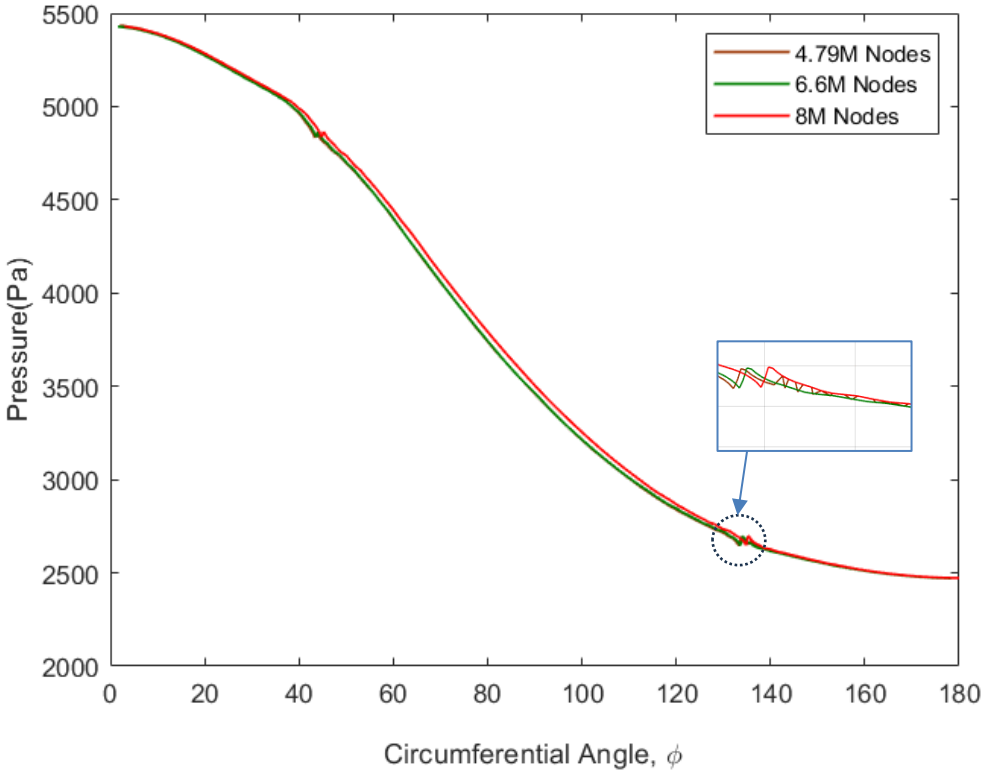

Fig 4. Comparison of Circumferential Surface Pressure distribution for different mesh size

The above results show that the three mesh predicts almost same value of circumferential pressure distribution over the cone except for the fact that there is little fluctuation near Φ=135° in circumferential surface pressure distribution for the coarse mesh. But the finer mesh is chosen as the definitive mesh since the convergence time between the mesh is not much of difference. In addition, the finer mesh will provide a better resolution when examining for higher angle of attack.

3.6 Validation

Figure 5 presents a comparison of the normalized circumferential heat flux distribution from the windward to leeward meridian at x/l = 0.175 for 4° angle of attack, obtained from the 8M mesh, with experimental measurements conducted by Richard R. Tracey [3] over a 10° semi-apex angle cone for a freestream Mach number, static pressure, and temperature of 7.95, 190.73 Pa and 55.38 K respectively. Heat flux is normalized with heat flux at same position for 0° angle of attack. The agreement between the Laminar CFD model and the experimental Cp data is notably good.

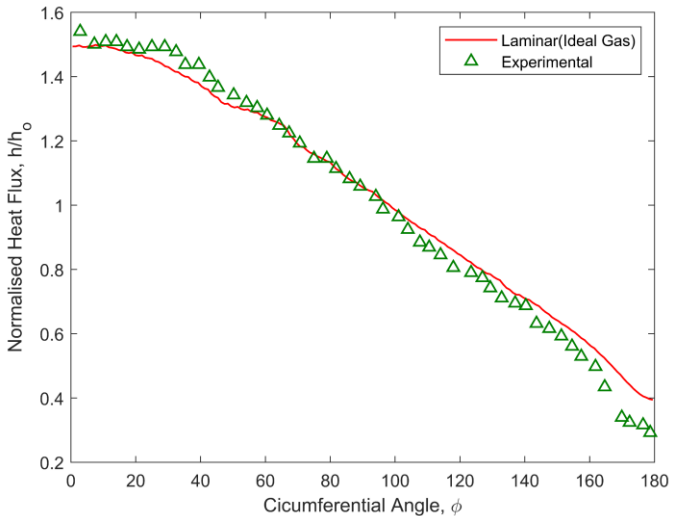

Fig 5. Circumferential Heat Flux distribution used for validation of the CFD model

4. Results and Discussion

The analysis encompasses data regarding the i. Pressure distribution comparison, ii. Circumferential heat flux variation, iii. Axial heat flux variation and iv. Heat flux to the cone base for each angle of attack case. For each case the free stream Mach Number and Stagnation Enthalpy is maintained as 6 and 1.1 MJ/Kg respectively. Measurements of circumferential heat flux were taken at designated positions along the cone, specifically referencing the 200mm cone model designated for experiments at the Hypersonic Experimental Aerodynamics Laboratory (HEAL), Indian Institute of Technology Kanpur. The specific x/L locations are 0.175, 0.2, 0.425 and 0.75 from the leading edge of the cone. The circumferential axis is referred to as Φ, where Φ = 0° is located at the windward meridian and Φ = 180° is at the leeward meridian.

4.1. Pressure Distribution Comparison

The results depicted in Fig 6.A illustrate the contour of pressure coefficient distribution with density contour lines at various angles of attack and at x/L = 0.425 position from the apex of the cone. At 0° angle of attack, the pressure contour exhibits a uniform pressure distribution across the entire cone surface due to formation of conical shock symmetric about the axis of the cone. However, as the angle of attack increases, there is a noticeable rise in pressure on the windward side of the cone. This can be attributed to the increase in shock strength due to the increase in flow deflection angle from 12° to 16° for α = 4° and α = 8° respectively. Fig 6.B reveals the formation of shockwaves resulting from the deflection of flow, particularly evident at higher angles of attack. At an angle of 8°, no shockwave is observed on the top surface of the cone as the flow aligns with the surface. Additionally, downstream of the flow field, a distinct recirculation zone emerges near the base of the cone due to abrupt expansion fan occurring at the shoulder of the cone.

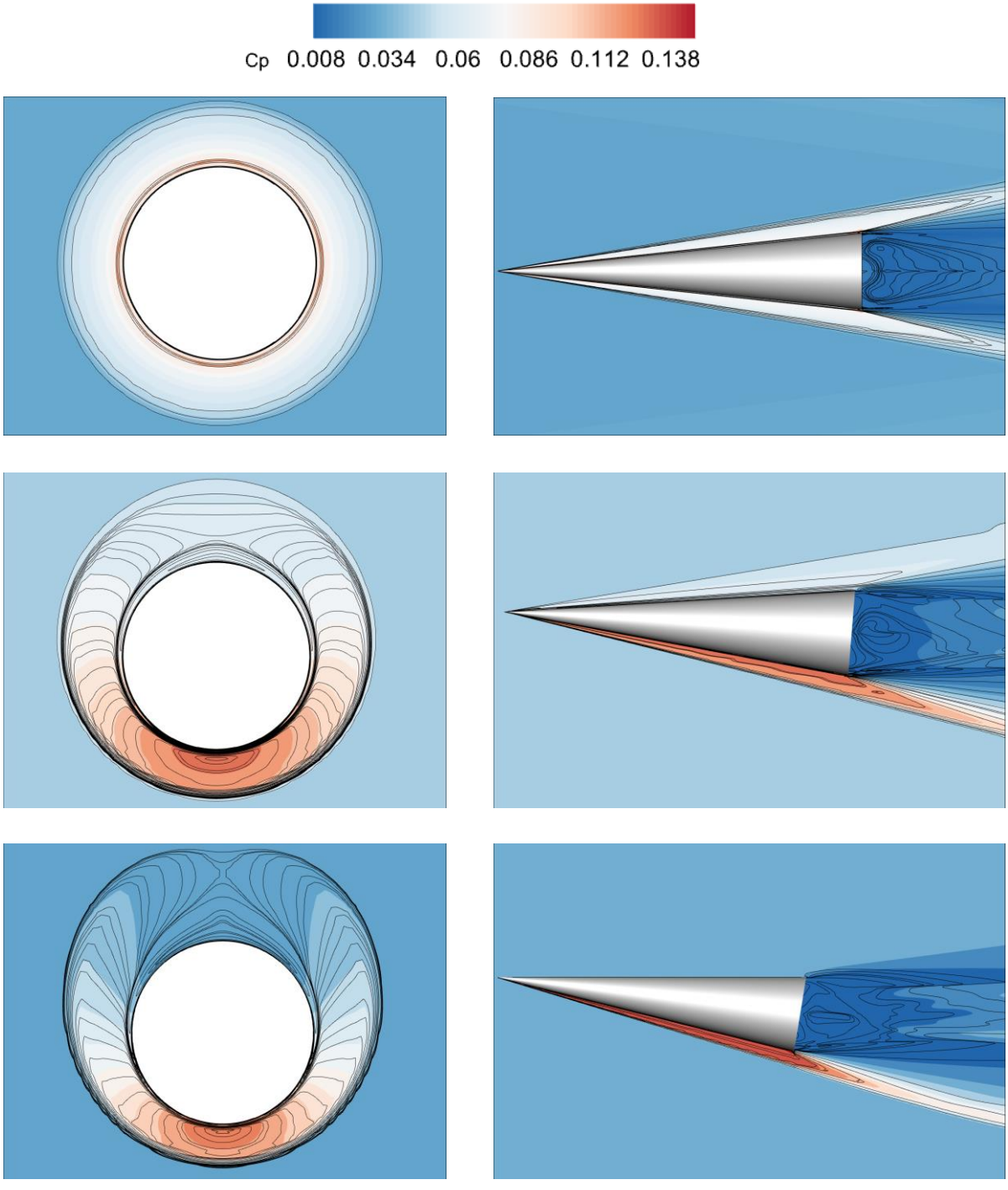

Fig 6. A. Circumferential C_p distribution with density contour lines for α = 0°, α = 4° and α = 8° (upper row to lower row) at x/L = 0.175; B. Axial C_p distribution with density contour lines for α = 0°, α = 4° and α = 8° (upper row to lower row)

4.2. Circumferential Heat Flux Variation

Fig 7 illustrates the variation of circumferential heat flux with respect to the circumferential axis. In Fig 7.A, the absolute values of circumferential heat flux are depicted, while in Fig 7.B and 7.C, the values are normalized using the heat flux at 0.175L for 0° angle of attack. For 0° angle of attack, the circumferential heat flux remains nearly constant along Φ at a specific distance from the cone's apex, reflecting the symmetry of flow about the cone's axis. Similarly, the pattern of variation is consistent for angles of attack of 4° and 8°, with maximum heat flux observed at the windward meridian and minimum heat flux at the leeward meridian. This variation is attributed to the increased shock strength on the windward meridian with higher angles of attack. However, the key distinction between 4° and 8° angles of attack lies in the rate at which heat flux decreases along the circumferential axis, with a more rapid decrease observed for 8° due to the more shock strength.

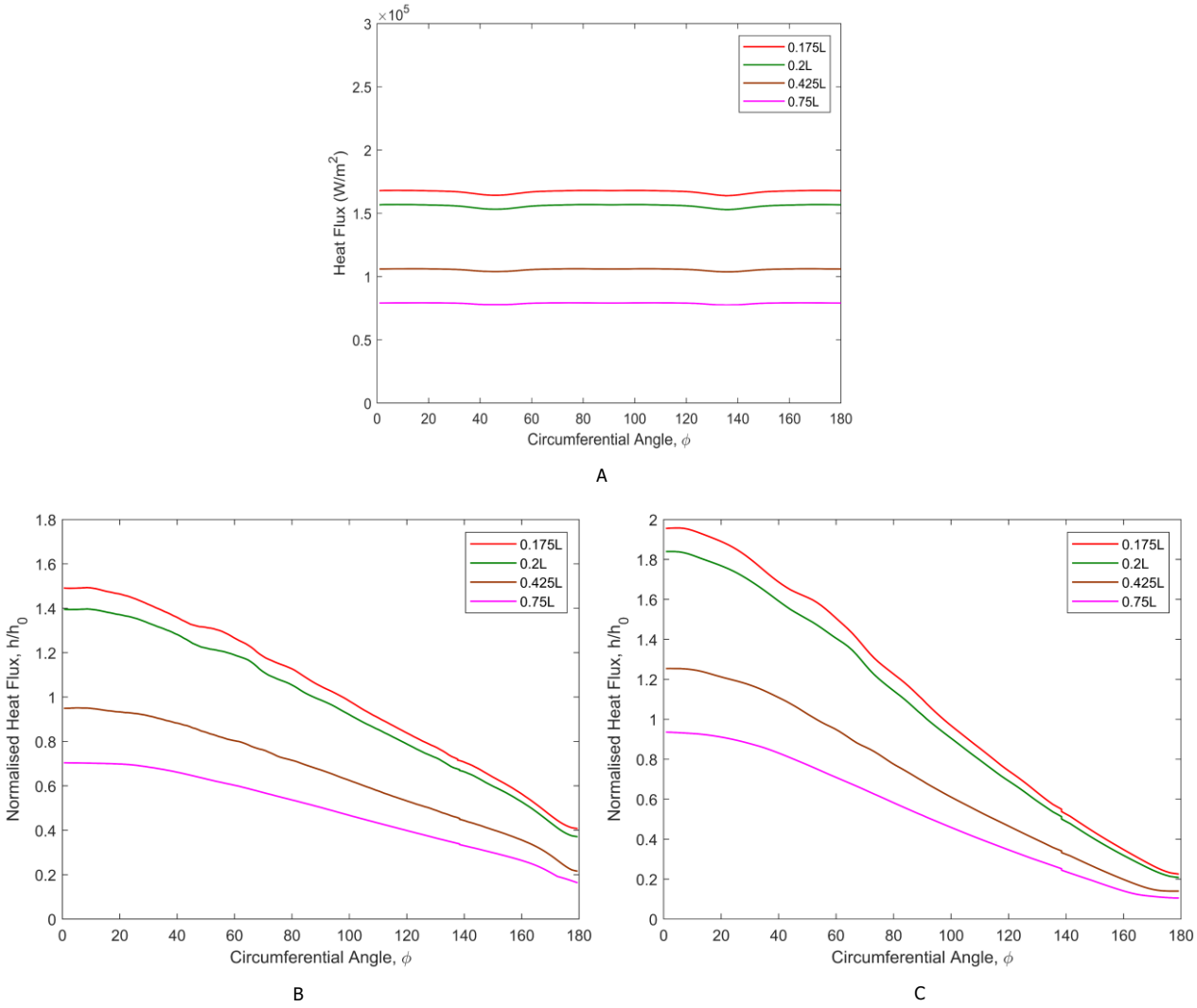

Fig 7. Circumferential Heat Flux Distribution for α = 0° (A), α = 4° (B) and α = 8° (C)

4.3. Axial Heat Flux Variation

The surface heat flux variation with X/L is shown in Fig 8. In 8.A the absolute value of heat flux is shown while for Fig 8.B and 8.C the heat flux is normalized by heat flux at 0.175L for 0° angle of attack. The following inference can be drawn from the plot: 1. The highest heat flux is concentrated near the tip of the cone, gradually diminishing in intensity as we move along the axial direction; 2. For 0° angle of attack the heat flux for the leeward surface and the windward surface coincides since the flow is symmetric along the entire length of the cone. 3. For 4° and 8° angle of attack, the heat flux distribution on the windward surface of the cone is more as compared to the leeward surface of the cone. This is mainly due to an increase in flow deflection angle on the windward meridian with increase in α. Due to increased shock strength, the rise in temperature will result in more heat flux to the windward surface of the cone. The maximum heat flux is at the tip of the cone due to the maximum temperature difference between the flow just after the shock and the surface. It can be seen that the heat flux decreases axially. This is due to a decrease in the temperature difference between the surface and the high temperature flow.

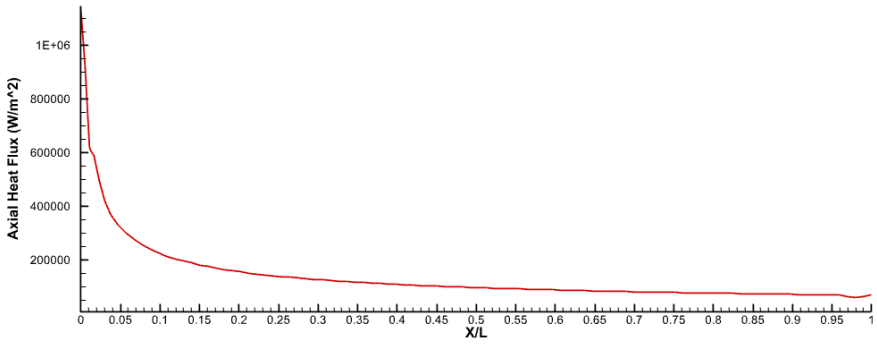

A

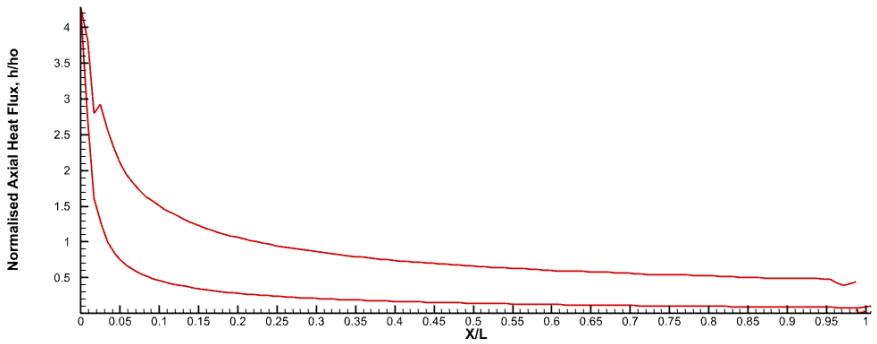

B

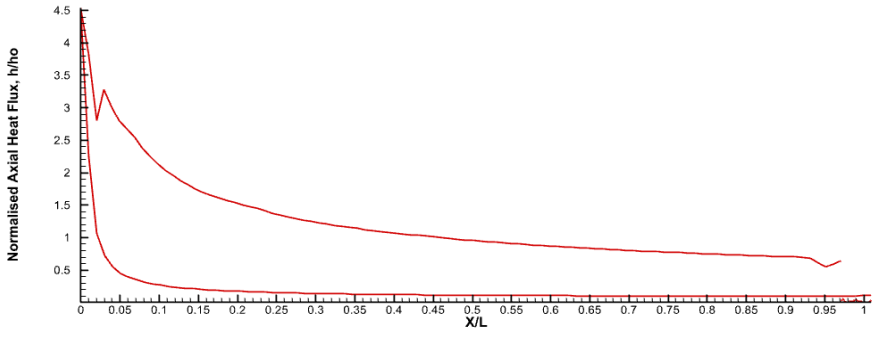

C

Fig 8. Axial Heat Flux Distribution for α = 0° (A), α = 4° (B) and α = 8° (C)

4.4. Cone Base Heat Flux Distribution

The heat flux at the base of the cone is shown in Fig 9. For α = 0°, the heat flux rises due to the recirculation zone created at the center of the base of the cone due to symmetric expansion fan over the entire periphery of the base. This pattern is created since the flow symmetrically enters the base of the cone from all sides. In addition to that, a source is also noted at the center of the base which can be attributed as the projection of a 3D recirculation region present at that spot. For α = 4°, there are two circulation zones from where the streamlines diverge due to formation of 3D recirculation zone. A circular pattern appears to form due to interaction between the recirculation zone and the incoming streamline emerging from the periphery of the base. On increasing the angle of attack to α = 8°, the strength of the recirculation zone on the leeward side of the cone base decreases due to more expansion. This can be attributed from decrement in heat flux towards the top of the base. This also results in shifting of local peaks of heat flux towards the leeward side, which were initially present below the centerline of the base for α = 4°.

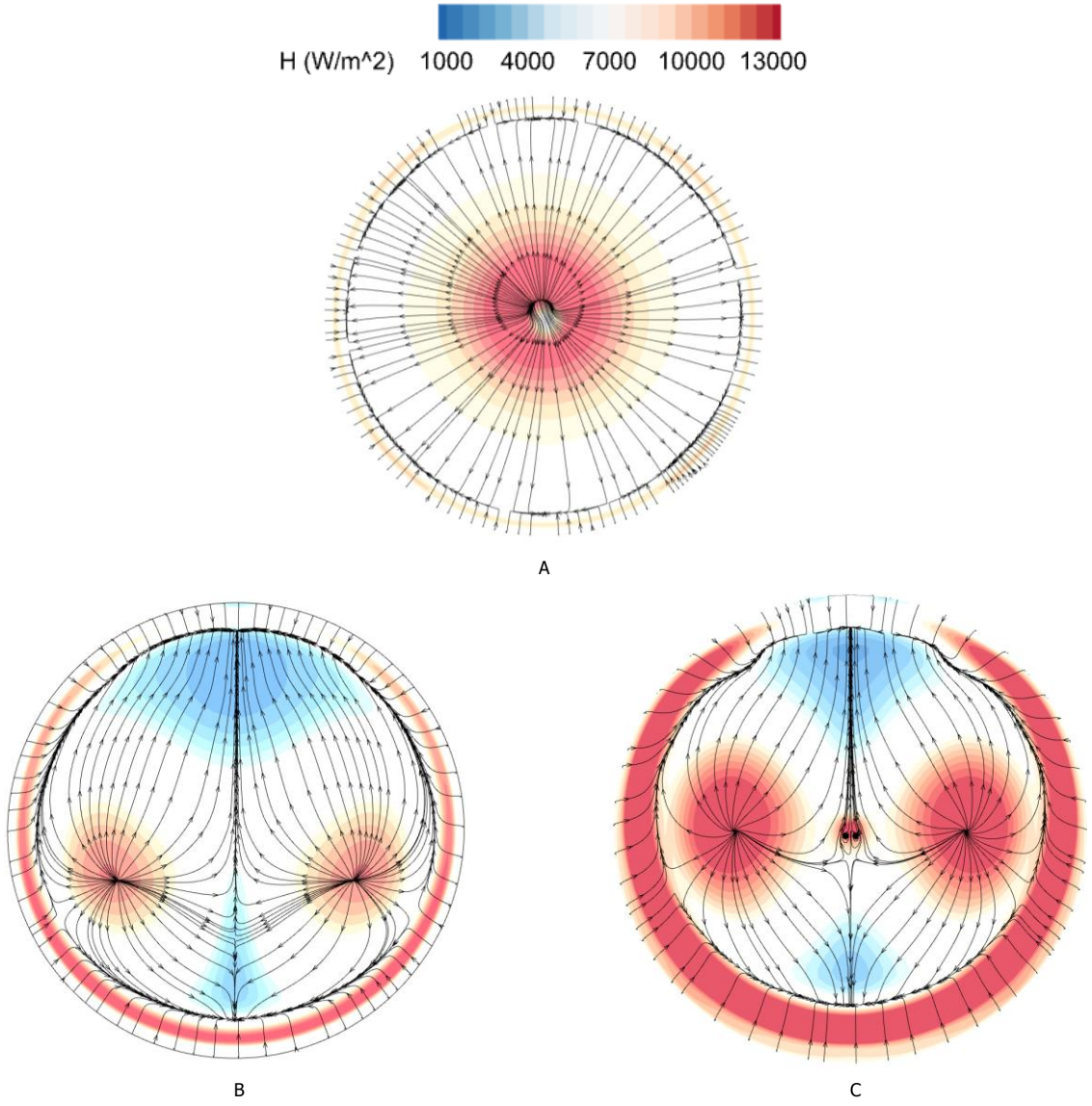

Fig 9. Base Heat Flux Distribution for α = 0° (A), α = 4° (B) and α = 8° (C)

5. Conclusion

The conclusions derived from numerical study of flow over a 3D cone at three angles of attacks are as follows:

- Laminar flow model with perfect gas assumptions can be used to resolve the heat transfer data for low angle of attacks up to 8°.
- At α = 0°, the heat flux on both the leeward and windward sides of the cone exhibit a consistent pattern. However, as the angle of attack increases, the heat flux on the windward surface becomes more dominant than that on the leeward surface.
- The heat flux in the axial direction is maximum near the tip of the cone which gradually decreases towards the base of the cone.
- For 0<α<= 8°, the heat flux pattern on the base of the cone remains consistent, with a gradual shift in the position of the predominant recirculation zone toward the leeward meridian.
- With increase in angle of attack, there will be flow separation and the recirculation zones at the base of the cone will increase in volume. So, a turbulent model must be employed to resolve the flow.
- Work is still in progress for High Enthalpy Flow. To validate the results, experiments will be conduct in Hypersonic Experimental Aerodynamics Laboratory (HEAL), IIT Kanpur, India.

6. Acknowledgement

I would like to express my sincere gratitude to the High-Performance Computing Facility at the Indian Institute of Technology Kanpur for providing the computational resources necessary to conduct the simulations presented in this research.

7. References

[1] Einar Karl T. Carias and Simon A. Prince, "Validation study of blunted and sharp cones at hypersonic speed": In ICAS 2022.

[2] Maccoll, JW. The conical shock wave formed by a cone moving at a high speed. The Royal Society of London. Series A-Mathematical and Physical Sciences, 159(898):459–472, 1937.

[3] Tracey, Richard R. Hypersonic Flow over a Yawed Circular Cone. Hypersonic Research Project Memorandum, page 15, 1963.

[4] Rasmussen, Maurice L. On hypersonic flow past an unyawed cone. AIAA Journal, 5(8):1495–1497, 1967.

[5] Ferri, Antonio. Supersonic flow around circular cones at angles of attack. Technical report, 1951.

[6] Stone, AH. On supersonic flow past a slightly yawing cone. Journal of Mathematics and Physics, 27(1-4):67–81, 1948.

[7] Van Dyke, Milton D. A study of hypersonic small disturbance theory. Technical report, 1954.

[8] Sims, Joseph L. Tables for supersonic flow around right circular cones at small angle of attack, volume 3007. Scientific and Technical Information Division, National Aeronautics and Space, 1964.

[9] Kopal, Zdenek. ˇ Tables of supersonic flow around yawing cones. Massachusetts Institute of Technology, 1947.

[10] Cheng, HK. Hypersonic flows past a yawed circular cone and other pointed bodies. Journal of Fluid Mechanics, 12(2):169–191, 1962.

[11] Doty, Roberto T and Rasmussen, Maurice L. Approximation for hypersonic flow past an inclined cone. AIAA Journal, 11(9):1310–1315, 1973.

[12] Versteeg, Henk Kaarle and Malalasekera, Weeratunge. An introduction to computational fluid dynamics: the finite volume method. Pearson education, 2007.

[13] John D. Anderson Jr. Hypersonic and High Temperature Gas dynamics

[14] Adriana McDonald Tariang. A Study on Hypersonic Flow Over Atmosphere Entry Configurations